



## Analytical note

## Matrix effects on laser-induced plasma parameters for soils and ores

Andrey M. Popov<sup>a,\*</sup>, Sergey M. Zaytsev<sup>a</sup>, Irina V. Seliverstova<sup>a</sup>, Alexander S. Zakuskin<sup>a</sup>, Timur A. Labutin<sup>a,b</sup>

<sup>a</sup> Department of Chemistry, Lomonosov Moscow State University, 119234, Leninskie Gory, Moscow, Russia

<sup>b</sup> Shirshov Institute of Oceanology, Russian Academy of Sciences, 117997, Nakhimovsky Prospekt, Moscow, Russia



## ARTICLE INFO

## Keywords:

Geomaterials  
Compressive force  
Moisture  
Easily ionized element

## ABSTRACT

Matrix effects caused by either physical properties or chemical nature of a sample are the main analytical problems of laser-induced breakdown spectroscopy responsible for worsening of accuracy. We have studied a relation of laser plasma parameters and three intrinsic properties of powders for soils and ores: (i) sample moisture content; (ii) compressive force for sample pelleting; (iii) total content of easily ionized elements (EIEs). We prepared three sets of soils (calcareous, black, and sod-podzol) with different moisture content (from 0% to 8% wt.) by saturation of dried powders with water vapor. Moisture of soils did not influence plasma temperature and its electron density, while the intensity of particular emission line (Mn I 403.08 nm) had two opposite trends for the black and sod-podzol soils, decreasing with moisture content, and increasing for the gray calcareous soil. The latter seems to be due to cementation of Ca-rich soil. A fine-dispersed powder of ferromanganese nodules was compressed by application of compressive force ranged in 0–10 tons/cm<sup>2</sup> to investigate its influence on plasma parameters. Electron density increased in several times with the growth of compressive force that was mostly expressed at longer delays (7.5 μs). Although the compressive force had not such a strong influence on plasma temperature, we demonstrated that a short delay (0.5–1 μs) provided minimal changes in plasma parameters. The variation of EIEs content (0.5–13% wt.) in the used certified samples allowed investigation of the EIEs effect. Electron density was similar for a relatively low content (< 5% wt.), while electron density increased in several times for high content of EIEs. Plasma temperature did not clearly depend on soil types or EIEs content. We concluded that EIEs content mostly influences on ionization equilibrium.

## 1. Introduction

Laser ablation of solid samples is accompanied with strong matrix effects due to the influence of physical and chemical properties of a sample on the laser-matter interaction or/and plasma-particles interaction [1–4]. The earliest study of laser induced plasma demonstrated a clear relationship between spectral line intensities of main components and recrystallization conditions, grain size, and mechanical strain of a material [5]. Later it was shown that the hardness of titanium alloys influences the ablation rate and, hence, the emission signal [6]. It is well-known that thermal properties in particular temperatures of phase transitions or melting and evaporation heats are strongly correlated with the vaporized volume of a sample as well as with the breakdown threshold [7]. A change in the breakdown threshold comes to be more appreciable for ablation of non-metal samples (e.g. ceramics) in contrast to ablation of metal alloys [8]. In addition, the thermal diffusivity at melting point of metals has a good correlation with a mass enhancement by double-pulse ablation, while melting temperature does

not correlate with the mass enhancement [9]. Moreover, the widely differing conditions of plasma ignition result in a strong variation of its evolution, and there are only few studies on the relation of plasma dynamics with ablation of pure metals using one-dimensional consideration in vacuum [10,11].

Since the general model for multicomponent sample, describing the processes from the initial stage of laser-matter interaction to plasma ignition and expansion, is absent, there are a number of studies on influence of a particular physical property of sample on plasma parameters. We have demonstrated the linear dependence of plasma temperature on microhardness of aluminum alloys [12,13]. Although hardness was correlated with ratio of ionic and atomic lines in Refs. [14,15], the more recent studies have demonstrated the advantages of plasma temperature to characterize hardness of materials [16–18]. It was also suggested to evaluate aging grade of steels [19] by lines intensity ratio. Liu et al. [20] have demonstrated the linear correlation between intensities of O I line and moisture of cheese, while Paris et al. [21] have found the inconsiderable effect of moisture content of

\* Corresponding author.

E-mail address: [popov@laser.chem.msu.ru](mailto:popov@laser.chem.msu.ru) (A.M. Popov).

<https://doi.org/10.1016/j.sab.2018.07.005>

Received 1 February 2018; Received in revised form 2 July 2018; Accepted 4 July 2018

Available online 06 July 2018

0584-8547/ © 2018 Elsevier B.V. All rights reserved.

limestone on plasma properties. Conversely, plasma electron density has clearly increased with cooling of rock samples to Martian conditions. This effect was assigned by Rauschenbach et al. [22] to ice cementation since intensities of O I and H I lines have non-monotonically changed near the triple point of water. Rapin et al. [23] have recently found that the rock roughness can only influence H I line intensities in contrast with stable intensity of O I, C I, Al I lines.

Variety of chemical forms of an element in a sample is another source of matrix effects. Eppler et al. [24] have demonstrated the following effect in case of soils and sands: the barium emission intensity has decreased in the order carbonate > oxide > sulfate > chloride > nitrate, while the lead one has varied in the order oxide > carbonate > chloride > sulfate > nitrate. We have recently [25] found the strong matrix effects for copper, lead and molybdenum emission signal originated from different types of soils and ores. Ablation rate of the pearlite/ferrite region of steel surface was distinctly larger than of the martensite one, whereas the values of plasma temperature were similar in both cases [26]. On the contrary, Pořízka et al. [27] have recently showed the linear increase of plasma temperature and electron density with the grade of Mg corrosion. Surface morphology also strongly influences plasma temperature, which was exemplified by signal difference between annealed and non-annealed samples of  $\alpha$ -LiFe<sub>5</sub>O<sub>8</sub> [28]. Thus it is quite difficult to find appropriate matrix-matched reference materials since all kinds of matrix effects act simultaneously. Some researchers have suggested the sample discrimination between groups [29] characterized by the certain properties.

Direct analysis of powders (ores, soils, ceramics, etc.) by laser ablation techniques is primarily influenced by cohesion of grains and granulometric composition of the samples. Several ways can be implemented to reduce these effects: (i) simple pelleting of dried powder [30], (ii) the use of binder in case of low cohesive strength of a material (such as sand) [31,32], (iii) placing powder onto the adhesive sticky tape [33]. Moreover, the last one was examined to compensate for matrix effects by the surface density normalization method [34]. Obviously, the packing density of pellets and powders on tape can be strongly varied, worsening the precision of analytical measurements [35].

The goal of this work is to estimate the influence of the sample properties, namely, compression force, moisture, and content of easily ionized elements (EIEs), on plasma temperature ( $T$ ) and electron density ( $N_e$ ). It would be fruitful to provide some recommendations on mitigation of matrix effects in the analysis of different types of soils, pelagic sediments, ores and nodules.

## 2. Experimental

### 2.1. Instruments

Experimental set-up is a typical instrument for laser-induced breakdown spectrometry (LIBS) including Q-switched Nd:YAG laser (LOTIS TII, 532 nm,  $E = 75$  mJ/pulse, 5 Hz). Two high-aperture 0.32 m Czerny-Turner spectrographs (HR-320) provide medium (10,000 at 540 nm with grating 1800 lines/mm, slit 25  $\mu$ m, system #1) and high resolution (22,000 at 405 nm with grating 3600 lines/mm, slit 25  $\mu$ m, system #2). A plasma light was collected by two-lens condenser (system #1) or by an aspheric quartz lens with short focus ( $f = 30$  mm) on to the entrance face of “line-to-line” fiber (82 cores with a diameter of 100  $\mu$ m) (system #2). Laser beam was focused ( $f = 150$  mm) perpendicularly to the sample (3 mm below the surface). System #1 was used for some measurements, because, despite the preferable higher resolution, system #2 had a red edge at 529.5 nm. Plasma emission spectra were recorded by intensified charge coupled device (Nanogeit-2V, Russia) with the use of laboratory-made software previously described elsewhere [36].

### 2.2. Samples under investigation

We used three types of samples. Ferromanganese nodule (OOPE604) is a certified reference material (CRM) of pelagic sediments to study the effect of compression force. OOPE604 contains the following main components: Fe (15.5% wt.), Mn (15.3% wt.) in MnO<sub>2</sub> form, Si (10.4%), Ca (3.67%), Al (3.55%), Na (1.66%), Mg (1.38%) and other elements with content lower than 1%. According to its Certificate, the material represents a fine-dispersed powder with the particle sizes lower than 30  $\mu$ m (> 80%). Since we used the same CRM to assess compression force effect, the obtained results are independent of the influence of granulometric and mineral composition of the sample, and, therefore, the found relationship can be relevant for other types of powdered samples (e.g. soils, ores). A set of pellets with diameter of 12 mm was prepared by the hydraulic press machine with compression force from 160 kg/cm<sup>2</sup> to 10 tons/cm<sup>2</sup>. A piece of sticky tape covered with the powder served as a non-pressed sample. We prepared three samples of soils (sod-podzol OOKO153, gray calcareous SSK3, black SCHK3) with different moisture grades to investigate moisture effect. We labeled raw CRMs as “medium” moisture grade and their moisture remained constant at room temperature. To calculate “medium” moisture content we dried the samples to constant weight at  $105 \pm 2$  °C. Maximal hygroscopic moisture content given in Supplementary Table S1 was determined for the soil samples in accordance with Russian standards [37]. A step-by-step description to prepare samples with different grades of moisture is given in Supplementary material. To study the impact of EIEs on plasma parameters we used a set of typical Russian soils and gold-bearing or copper-porphyry ores. Their composition is given in Supplementary Table S2 in accordance with their Certificates. Ore samples are poor in EIEs, simultaneously total content of EIEs in soils varies in the wide range. Before measurements, all powders were pressed in pellets under pressure of 1 ton/cm<sup>2</sup>.

### 2.3. Plasma diagnostics

Electron density of plasma was estimated by Stark widths of two lines: Fe I 538.34 nm for iron-manganese nodule and Sr II 407.77 nm for all other samples. We selected three values for Stark width of the iron line for different plasma temperature: 1.6 pm at  $N_e = 4 \times 10^{15}$  cm<sup>-3</sup> and  $T = 6600$  K, 56 pm for  $N_e = 3.25 \times 10^{16}$  cm<sup>-3</sup> and  $T = 9339$  K, and 78.8 pm for  $N_e = 2.82 \times 10^{16}$  cm<sup>-3</sup> and  $T = 13,019$  K among the values given by Lesage et al. [38]. We neglected the self-absorption of the line, following the recommendations by Aragón and Aguilera [39] for Fe-Si samples containing 40% iron vs 15.5% of iron in our nodule. Stark width of Sr II 407.77 nm was assumed to be equal to  $30 \pm 3$  pm for  $N_e = 10^{17}$  cm<sup>-3</sup> and  $T = 13,000$  K [40]. Since the content of strontium in soils and ores did not exceed 300 ppm, we neglected the line self-absorption. Both lines were fitted by Lorentz profile with instrumental widths of 55 pm (system #1) and 19 pm (system #2), respectively. Plasma temperature was estimated by two-lines method with the use of Mn I lines for soils and ores and Fe I lines for nodule. Typical spectra are shown in Supplementary Figs. S1 and S2 (Appendix). A list of identified lines and their parameters within two spectral ranges is given in Supplementary Table S3 (Appendix). We used the shortest possible gate (usually, gate-to-delay ratio was about 1:10 or lower) to achieve maximum accuracy in electron density and temperature calculation.

## 3. Results and discussion

### 3.1. Compressive force effect

Intensity of Fe I 532.42 nm line and its relative standard deviation (RSD) for 20 replicate measurements are presented as a function of compression force in Fig. 1. Measurements for the non-pressed sample were repeated only 5 times in 5 different points to avoid ablation of a

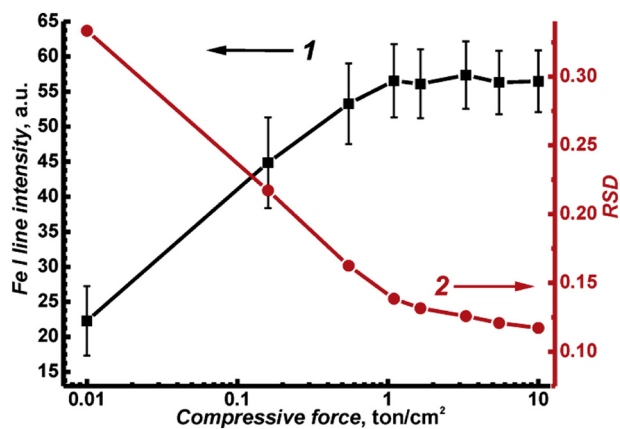


Fig. 1. Intensity of Fe I 532.42 nm line (1, left axis) and its RSD (2, right axis) as a function of compression force applied to the CRM of iron-manganese nodule. Delay 1.5  $\mu\text{s}$ , gate 100 ns. Error bars on curve 1 correspond to  $\pm \sigma$  (20 replicates).

sticky tape. Since the figure is plotted in logarithmic coordinate on x-axis, the value of 0.01 on x-axis corresponds to zeroth pressure. As one can see RSD (curve 2 in Fig. 1) decreases from 35% to 12% with growth of compression force, that is in agreement with the observations by Sivakumar et al. [35] for C-Fe mixtures. Since RSD trends like the dependence of tablet porosity on compressive force observed by Higuchi et al. [41], reasonable explanation is a change in distribution between empty space and particles for strongly pressed samples. Fe I line achieves maximal intensity (a plateau) in the range of 1–10 tons/cm<sup>2</sup> (curve 1 in Fig. 1), i.e. empty space between particles cannot be further reduced. In other words, particles of powdered material reach the closest packing as demonstrated by Li and Funkenbusch [42], which leads to an increase in the area occupied by the particles within a laser spot and, as a consequence, the intensity of emission signal. If we consider sample with other granulometric distribution, this plateau appears to be slightly shifted. Fig. 2 presents the evolution of plasma parameters observed for nodule pellets produced with different compression force. Similarly to Fig. 1, the value of 0.01 on x-axis corresponds to zeroth pressure. Since compressive force affects hardness of tablets [41] and hardness, in turn, correlates with plasma temperature [13,16], one can expect to observe a strong correlation between compression force and  $T$ . Unlike Fe I line intensity, we have not found such a clear dependence for temperature (Fig. 2, a) at different delays. In the same time,  $N_e$  obviously underwent the effect of sample compression (Fig. 2, b) with a linear dependence on compressive force below 1 ton/cm<sup>2</sup> in bilogarithmic coordinates. Thus electron density can be

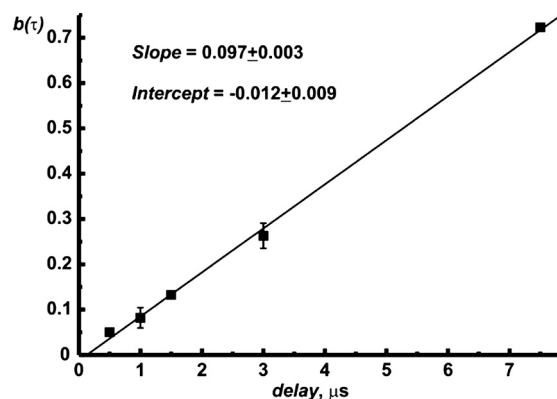


Fig. 3. Evolution of a power factor  $b$  for dependence of electron density and compressive force. Parameters of a line are shown in a legend. Error bars correspond to errors for approximation of  $N_e(\tau)$  by a power function of pressure.

represented as a power function of pressure  $N_e(\tau) = a(\tau) \times \text{pressure}^{b(\tau)}$ , where  $\tau$  is delay. A scale factor  $a(\tau)$  is a function of exponential decay that is common for evolution of electron density; while power factor  $b$  ( $\tau$ ) shows a linear function proportional to  $\tau/10 \mu\text{s}^{-1}$  (Fig. 3).

We can try to suggest some explanations of the observed effects. Certain pressure results in an apparent density of a sample  $\rho$  corresponding to mass of particles within a laser spot, i.e.  $\rho = \frac{1}{S_{\text{spot}}} \sum_{n=1}^N m_n$ , where  $S_{\text{spot}}$  is an area of laser spot,  $m_n$  is a  $n$ -th particle mass, and  $N$  is the number of particles. Obviously, the higher apparent density  $\rho_{\text{high}}$  of a sample with a strong compressive force applied results in an increase of total number  $N$  of particles within a spot (i.e.  $N(\rho_{\text{high}}) > N(\rho_{\text{low}})$ ). Assuming that the plasma volume at certain delay is dominantly determined by laser fluence, then the average atomic number density will be higher for  $\rho_{\text{high}}$ . The interesting conclusion may be made about ionization equilibrium: the part of Saha equation depending on plasma temperature  $T$  stays the same for different apparent densities, and, therefore, the growth of atomic number density ( $\rho_{\text{high}}$  vs  $\rho_{\text{low}}$ ) is compensated by the equal growth of  $N_e$ . Besides this, the variation in ablation threshold may be a reason of such a difference in the plasma parameters. If we assume that the probability of plasma ignition increases for a larger number of particles, the ablation threshold would be lower for denser samples. This leads to a greater laser absorption in the plasma by inverse Bremsstrahlung and, consequently, to higher plasma temperature and electron density [11]. The above speculations qualitatively describe the compressive force effect. This effect can be diminished by the plasma observation at short delays ( $< 1 \mu\text{s}$ ) that is clearly confirmed by the stable intensity of Fe I 532.42 nm line at short delay (Fig. 4).

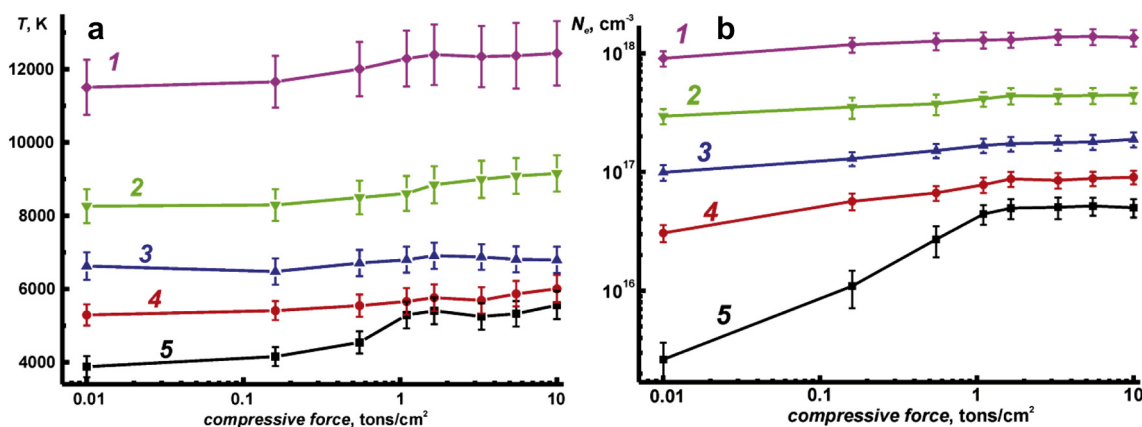


Fig. 2. Plasma temperature (a) and electron density (b) as a function of pressure applied to material of iron-manganese nodule at different delays and gates: 500 ns and 30 ns (1), 1  $\mu\text{s}$  and 50 ns (2), 1.5  $\mu\text{s}$  and 100 ns (3), 3  $\mu\text{s}$  and 100 ns (4), 7.5  $\mu\text{s}$  and 250 ns (5). Error bars correspond to  $\pm \sigma$  (20 replicates).

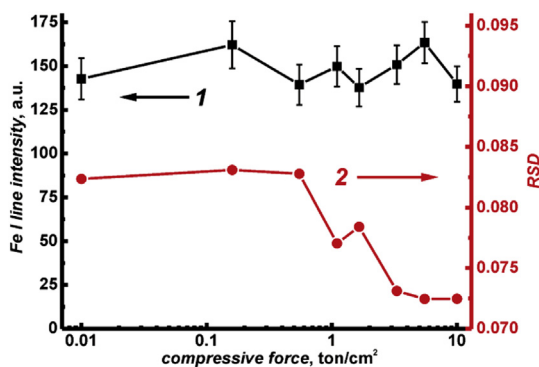


Fig. 4. Intensity of Fe I 532.42 nm line (1, left axis) and its RSD (2, right axis) as a function of compressive force applied to the material of iron-manganese nodule. Delay 500 ns, gate 30 ns. Error bars on curve 1 correspond to  $\pm \sigma$  (20 replicates).

### 3.2. Moisture effects

We used single spectral range (400–408 nm) for plasma diagnostics to avoid noticeable changes in moisture content of prepared samples during measurement procedure. Since Pb I 405.78 nm line was weak due to low gate-to-delay ratio of 1:10, we chosen manganese as a trace element. Note that manganese has a similar behavior in the soil to Zn and Cu, especially with respect to relative availability in acidic and alkaline soils [43]. Since Mn content in soils varied between 395 ppm and 690 ppm, its signal at 403.08 nm (Fig. 5) under certain temporal conditions was normalized to those for dried sample to compare the moisture effect for different soil types. In addition, such a procedure is helpful for trends comparison for different delays and gates. Sod-podzol soil (Fig. 5, a) and black soil (Fig. 5, b) demonstrated a decrease of signal for all delays, and the deeper drop was observed at the later stages of plasma lifetime. In the same way the intensities of Pb I line and Cu I line fell with growth of soil moisture in the recent study of Meng et al. [44]. Similar influence of moisture on the total intensities of oxygen triplet near 778 nm and CN band was observed by Liu et al. [20] for cheese samples. Contrary, the intensity of manganese line increased with the moisture content of gray calcareous soil (Fig. 5, c). Again the impact was stronger for the longer delay times. Such trend was also observed earlier by Paris et al. [21] for C I line at 247.86 nm in case of limestone and oil shales. Thus, moisture content has mixed effects on the line intensities, which, apparently, is due to differences in particles cohesion, cementation and the form of the elements for various soil types. A reduced soil cohesion at high moisture content [45,46] leads to decrease of the total number of particles in a volume unit, and, therefore, of ablated amount of analyte. On the contrary, gray calcareous soil is worse pelleted (especially dry powder) than other samples, and moisture can be considered as a “binding agent” due to interaction of calcium carbonate with water [47]. Increased cohesion at water content

up to 8–12% [48] raised the quantity of ablated mass.

To specify a reason for the moisture effect, we studied evolution of plasma parameters obtained at different grades of moisture (Fig. 6). Delays and gates were the same as those in Fig. 5. The parameters were the same within error bars, thus, neither  $N_e$  nor  $T$  depended on moisture content. These observations correlate with previous findings by Paris et al. [21], showing that plasma parameters do not change with moisture content increase from 0% (limestone) to 2.5% (oil shales). Moreover, the plasma temperature (Fig. 6, b) was actually the same for all samples with insignificant decay (within errors of temperature calculation) at the longest delay. Unlike temperature,  $N_e$  decreased from calcareous soil to sod-podzol soil. Initial electron density rose with content of EIEs (see Supplementary Table S1). Actually, gray calcareous soils contain a lot of calcium and magnesium unlike sod-podzol soil or black soil. Since slopes of each curves were practically the same (about  $-1.6$  in log-log coordinates), one can assume a close plasma expansion rate for all samples. Since there are no clear effects of moisture content on plasma parameters, while LIBS signal varies, we can suggest that the changes of soil cohesion results, in the first turn, in the changes of ablated atoms number per volume unit, but not in plasma parameters which seem to be related with laser fluence only.

### 3.3. EIEs effect

Since we found the influence of calcium content on electron density of plasma, we have thoroughly studied an influence of EIEs on plasma parameters for a set of soil and ore samples (see Supplementary Table S2). In Fig. 7 electron density and plasma temperature are shown as a function of total content of EIEs in the sample. Obviously, EIEs effect on electron density of laser-induced plasma became valuable only for their high total content ( $> 5\%$  wt.) because other main components of soils (such as aluminum, iron, titanium, etc.) can also produce electrons in typical plasma conditions. For example, Al has an ionization potential of 5.99 eV, which is slightly lower than one for calcium (6.12 eV). For convenience, we added a linear trend for the EIE's content  $> 4\%$ , while a horizontal line was used in Fig. 7 below this concentration. The strong growth of  $N_e$  for samples with high EIEs content can be related to their complete ionization under our experimental conditions. We have previously observed [49] similar trend in case of solutions of sodium chloride in water. Such an additive is known as an *ionization buffer*, which is added to increase free-electron concentration in plasmas, and its application for stabilizing the degree of ionization is a common practice for analysis by ICP-OES, flame photometry or atomic absorption techniques. For example, additions of lithium also provided the growth of plasma electron density in inductively-coupled plasma [50]. Summarizing above discussions, variations of  $N_e$  should be kept in mind to compensate them. Conversely, the plasma temperature (Fig. 7, b) slightly varied with total content of EIEs. The NIST 2710a datum is a clear outlier because of a high content of manganese in the sample (2140 ppm), resulted in self-absorption of Mn I lines and, therefore,

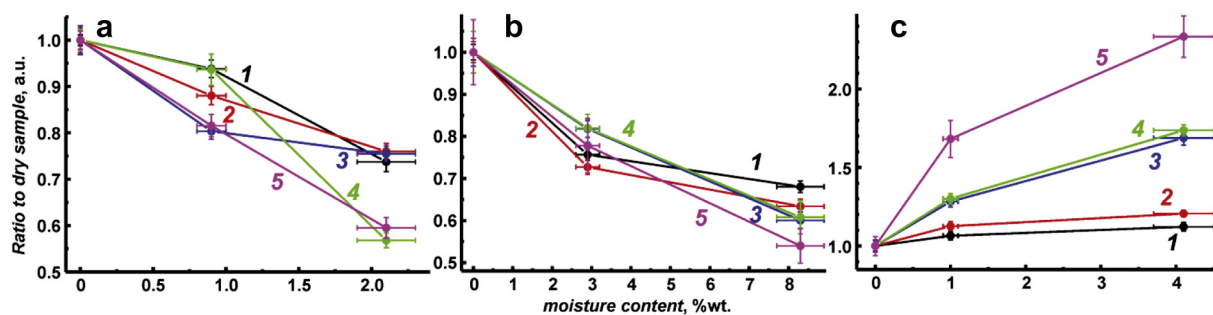


Fig. 5. Ratio of Mn I 403.08 nm for sample with certain grade of moisture to the same line for dried sample (moisture content 0%) as a function of moisture content for three samples: sod-podzol soil (OOKO153, a), black soil (SCHT3, b) and gray calcareous soil (SSK3, c), for different delays and gates: 0.5  $\mu$ s and 50 ns (1), 0.75  $\mu$ s and 50 ns (2), 1  $\mu$ s and 100 ns (3), 1.5  $\mu$ s and 150 ns (4), and 2  $\mu$ s and 200 ns (5). Error bars correspond to  $\pm \sigma$  (20 replicates).

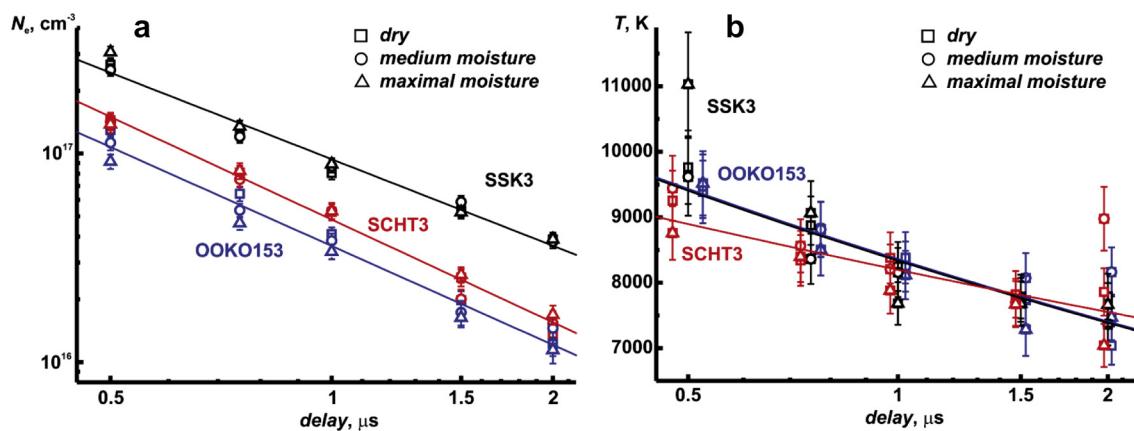


Fig. 6. Evolution of electron density (a) and plasma temperature (b) for three soil samples (SSK3 – black symbols, SCHT3 – red symbols, OOKO153 – blue symbols) with three grades of moisture: open squares correspond to dry samples, open circles correspond to medium moisture, open triangles correspond to maximal moisture. To illustrate closeness between values of plasma temperature, the delays for SCHT3 and OOKO153 are shifted by  $-25\text{ ns}$  and  $+25\text{ ns}$ , respectively. Error bars correspond to  $\pm \sigma$  (20 replicates). (For interpretation of the references to color in this figure legend, the reader is referred to the web version of this article.)

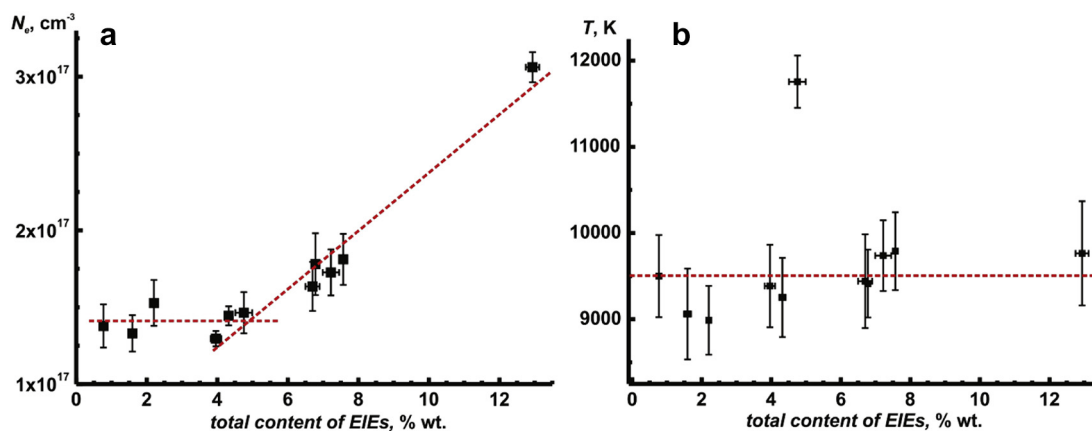


Fig. 7. Correlation of electron density (a) and plasma temperature (b) with total content of EIEs in soils and ores. Delay time 500 ns, gate 50 ns. Red dashed lines are trends for plasma parameters. Error bars correspond to  $\pm \sigma$  (20 replicates). (For interpretation of the references to color in this figure legend, the reader is referred to the web version of this article.)

overestimation of the plasma temperature.

#### 4. Conclusions

We have investigated the effect of compression force, moisture, and total content of EIEs on plasma parameters and intensity of analytical signals for different types of geomaterials. Hygroscopic moisture content influences the intensity of certain lines, while the plasma parameters remain approximately the same. It is also important that the effect on intensity is positive or negative for different soil types. Therefore, it seems reasonable to dry soil samples for hygroscopic moisture removal for better accuracy. A dramatic change of electron density with content of EIEs and the applied compression force was found. If EIEs simply produce more free electrons, the relationship between compression force and plasma parameters is quite different. It is interesting that the impact of a compression degree of powdered material intensifies at later period of plasma observation (at longer delays). The growth of electron density shifts an ionization equilibrium:  $X + \text{EIE}^+ \leftrightarrow X^+ + \text{EIE}$  from ionized analyte species to neutral ones. Thus, firstly, the earliest possible period of plasma observation can be recommended to minimize variations of plasma parameters (including emission intensity) due to the changes in compression effects especially for hardy pressed powders. Secondly, correction of moisture effect will be under further investigations because of dramatic changes of line intensities. Thirdly, a simple procedure providing with a preliminary

information about total content of EIEs (and possible types of soil) can be proposed: relatively high level of electron density (about  $3 \times 10^{17}\text{ cm}^{-3}$  at 500 ns) can be attributed to calcareous soils.

#### Acknowledgment

Dr. Andrey M. Popov thanks Russian Foundation for Basic Research and Moscow City Government for financial support of his contribution to the current work (Project no. 15-33-70055 “mol\_a\_mos”).

#### Appendix A. Supplementary data

Supplementary data to this article can be found online at <https://doi.org/10.1016/j.sab.2018.07.005>.

#### References

- [1] D.W. Hahn, N. Omenetto, Laser-Induced Breakdown Spectroscopy (LIBS), part II: review of instrumental and methodological approaches to material analysis and applications to different fields, *Appl. Spectrosc.* 66 (2012) 347–419.
- [2] R.E. Russo, X. Mao, J.J. Gonzalez, V. Zorba, J. Yoo, Laser ablation in analytical chemistry, *Anal. Chem.* 85 (2013) 6162–6177.
- [3] S. Zhang, M. He, Z. Yin, E. Zhu, W. Hang, B. Huang, Elemental fractionation and matrix effects in laser sampling based spectrometry, *J. Anal. At. Spectrom.* 31 (2016) 358–382.
- [4] T. Takahashi, B. Thornton, Quantitative methods for compensation of matrix effects and self-absorption in LIBS signals of solids, *Spectrochim. Acta B* 138 (2017) 31–42.

- [5] E. Cerrai, R. Trucco, On the matrix effect in laser sampled spectrochemical analysis, *Energia Nucleare* 15 (1968) 581–587.
- [6] V.V. Gusarskii, Yu. Ya, K.A. Kuzyakov, L.N. Timofeeva Semenenko, Some problems of the interaction of laser radiation with titanium alloys, *J. Appl. Spectrosc.* 31 (1979) 1224–1228.
- [7] L.M. Cabalin, J.J. Laserna, Experimental determination of laser induced breakdown thresholds of metals under nanosecond Q-switched laser operation, *Spectrochim. Acta B* 53 (1998) 723–730.
- [8] A.M. Popov, T.A. Labutin, A.E. Goldt, O.V. Usovich, S.E. Bozhenko, N.B. Zorov, Determination of lithium in lithium-ionic conductors by laser-enhanced ionization spectrometry with laser ablation, *J. Anal. At. Spectrom.* 29 (2014) 176–184.
- [9] G. Cristoforetti, S. Legnaioli, V. Palleschi, A. Salvetti, E. Tognoni, Effect of target composition on the emission enhancement observed in Double-Pulse Laser-Induced Breakdown Spectroscopy, *Spectrochim. Acta B* 63 (2008) 312–323.
- [10] E.A. Ershov-Pavlov, K.Yu. Katsalop, K.L. Stepanov, Yu.A. Stankevich, Time-space distribution of laser-induced plasma parameters and its influence on emission spectra of the laser plumes, *Spectrochim. Acta B* 63 (2008) 1024–1037.
- [11] A. Bogaerts, Zh. Chen, D. Autrique, Double pulse laser ablation and laser induced breakdown spectroscopy: a modeling investigation, *Spectrochim. Acta B* 63 (2008) 746–754.
- [12] T.A. Labutin, A.M. Popov, D.N. Sychev, N.B. Zorov, Correlation between mechanical properties of aluminum alloys and characteristics of laser-induced plasma, *Proc. SPIE* 7022 (2008) 70221C.
- [13] T.A. Labutin, A.M. Popov, V.N. Lednev, N.B. Zorov, Correlation between properties of a solid sample and laser-induced plasma parameters, *Spectrochim. Acta B* 64 (2009) 938–949.
- [14] K. Tsuyuki, S. Miura, N. Idris, K.H. Kurniawan, T.J. Lie, K. Kagawa, Measurement of concrete strength using the emission intensity ratio between Ca(II) 396.8 nm and Ca (I) 422.6 nm in a Nd:YAG laser-induced plasma, *Appl. Spectrosc.* 60 (2006) 61–64.
- [15] S. Yao, M. Dong, J. Lu, J. Li, X. Dong, Correlation between grade of pearlite spheroidization and laser induced spectra, *Laser Phys.* 23 (2013) 125702.
- [16] J.S. Cowpe, R.D. Moorehead, D. Moser, J.S. Astin, S. Karthikeyan, S.H. Kilcoyne, G. Crofts, R.D. Pilkington, Hardness determination of bio-ceramics using laser-induced breakdown spectroscopy, *Spectrochim. Acta B* 66 (2011) 290–294.
- [17] S. Messaoud Aberkane, A. Bendib, K. Yahiaoui, S. Boudjemai, S. Abdelli-Messaci, T. Kerdja, S.E. Amara, M.A. Harith, Correlation between Fe–V–C alloys surface hardness and plasma temperature via LIBS technique, *Appl. Surf. Sci.* 301 (2014) 225–229.
- [18] S. Messaoud Aberkane, A. Bendib, K. Yahiaoui, S. Abdelli-Messaci, S.E. Amara, M.A. Harith, Effect of laser wavelength on the correlation between plasma temperature and surface hardness of Fe–V–C metallic alloys, *Spectrochim. Acta B* 113 (2015) 147–151.
- [19] J. Li, J. Lu, Y. Dai, M. Dong, W. Zhong, S. Yao, Correlation between aging grade of T91 steel and spectral characteristics of the laser-induced plasma, *Appl. Surf. Sci.* 346 (2015) 302–310.
- [20] Y. Liu, L. Gigant, M. Baudelet, M. Richardson, Correlation between laser-induced breakdown spectroscopy signal and moisture content, *Spectrochim. Acta B* 73 (2012) 71–74.
- [21] P. Paris, K. Piip, A. Lepp, A. Lissovski, M. Aints, M. Laan, Discrimination of moist oil shale and limestone using laser induced breakdown spectroscopy, *Spectrochim. Acta B* 107 (2015) 61–66.
- [22] I. Rauschenbach, V. Lazic, S.G. Pavlov, H.-W. Hübers, E.K. Jessberger, Laser induced breakdown spectroscopy on soils and rocks: influence of the sample temperature, moisture and roughness, *Spectrochim. Acta B* 63 (2008) 1205–1215.
- [23] W. Rapin, B. Bousquet, J. Lasue, P.-Y. Meslin, J.-L. Lacour, C. Fabre, R.C. Wiens, J. Frydenvang, E. Dehouck, S. Maurice, O. Gasmault, O. Forni, A. Cousin, Roughness effects on the hydrogen signal in laser-induced breakdown spectroscopy, *Spectrochim. Acta B* 137 (2017) 13–22.
- [24] A.S. Eppler, D.A. Cremers, D.D. Hickmott, M.J. Ferris, A.C. Koskelo, Matrix effects in the detection of Pb and Ba in soils using laser-induced breakdown spectroscopy, *Appl. Spectrosc.* 50 (1996) 1175–1181.
- [25] A.M. Popov, T.A. Labutin, S.M. Zaytsev, I.V. Seliverstova, N.B. Zorov, I.A. Kal'ko, Y.N. Sidorina, I.A. Bugaev, Y.N. Nikolaev, Determination of Ag, Cu, Mo and Pb in soils and ores by laser-induced breakdown spectrometry, *J. Anal. At. Spectrom.* 29 (2014) 1925–1933.
- [26] S. Yao, J. Lu, K. Chen, S. Pan, J. Li, M. Dong, Study of laser-induced breakdown spectroscopy to discriminate pearlitic/ferritic from martensitic phases, *Appl. Surf. Sci.* 257 (2011) 3103–3110.
- [27] P. Pořízka, I. Ročňáková, J. Klus, D. Prochazka, L. Sládková, P. Šperka, Z. Spotz, L. Čelko, K. Novotný, J. Kaiser, Estimating the grade of Mg corrosion using laser-induced breakdown spectroscopy, *J. Anal. At. Spectrom.* 30 (2015) 2099–2106.
- [28] A.M. Popov, T.A. Labutin, V.V. Litvinova, N.B. Zorov, Influence of ferrite surface microstructure on laser ablation, *Proc. SPIE* 7022 (2008) 70221D.
- [29] P. Pořízka, A. Demidov, J. Kaiser, J. Keivanian, I. Gornushkin, U. Panne, J. Riedel, Laser-induced breakdown spectroscopy for in situ qualitative and quantitative analysis of mineral ores, *Spectrochim. Acta B* 101 (2014) 155–163.
- [30] A.M. Popov, M.O. Kozhnov, S.M. Zaytsev, N.B. Zorov, T.A. Labutin, Enhanced sensitivity of the direct beryllium determination in soil by laser-induced breakdown spectrometry, *J. Appl. Spectrosc.* 82 (2015) 739–743.
- [31] L. Shi, Q. Lin, Y. Duan, A novel specimen-preparing method using epoxy resin as binding material for LIBS analysis of powder samples, *Talanta* 144 (2015) 1370–1376.
- [32] S. Yao, J. Zhao, J. Xu, Z. Lu, J. Lu, Optimizing the binder percentage to reduce matrix effects for the LIBS analysis of carbon in coal, *J. Anal. At. Spectrom.* 32 (2017) 766–772.
- [33] S.C. Jantzi, J.R. Almirall, Elemental analysis of soils using laser ablation inductively coupled plasma mass spectrometry (LA-ICP-MS) and laser-induced breakdown spectroscopy (LIBS) with multivariate discrimination: tape mounting as an alternative to pellets for small forensic transfer specimens, *Appl. Spectrosc.* 68 (2014) 963–974.
- [34] S.I. Gornushkin, I.B. Gornushkin, J.M. Anzano, B.W. Smith, J.D. Winefordner, Effective normalization technique for correction of matrix effects in Laser-Induced Breakdown Spectroscopy detection of magnesium in powdered samples, *Appl. Spectrosc.* 56 (2002) 433–436.
- [35] P. Sivakumar, L. Taleh, Y. Markushin, N. Melikechi, Packing density effects on the fluctuations of the emission lines in laser-induced breakdown spectroscopy, *Spectrochim. Acta B* 92 (2014) 84–89.
- [36] S.M. Zaytsev, A.M. Popov, N.B. Zorov, T.A. Labutin, Measurement system for high-sensitivity LIBS analysis using ICCD camera in LabVIEW environment, *J. Instrum.* 9 (2014) P06010.
- [37] **Soils. Methods for determination of moisture, maximum hygroscopic moisture and moisture of sustainable wilting of plants, GOST 28268-89 (in Russian).**
- [38] A. Lesage, J.L. Lebrun, J. Richou, Temperature dependence of Stark parameters for Fe I lines, *Astrophys. J.* 360 (1990) 737–740.
- [39] C. Aragón, J.A. Aguilera, Determination of the local electron number density in laser-induced plasmas by Stark-broadened profiles of spectral lines: comparative results from H $\alpha$ , Fe I and Si II lines, *Spectrochim. Acta B* 65 (2010) 395–400.
- [40] C. Fleurier, S. Sahal-Brechot, J. Chapelle, Stark profiles of some ion lines of alkaline earth elements, *J. Quant. Spectrosc. Radiat. Transf.* 17 (1977) 595–604.
- [41] T. Higuchi, A.N. Rao, J.W. Busse, J.V. Swintosky, The physics of tablet compression. II. The influence of degree of compression on properties of tablets, *J. Am. Pharm. Assoc.* 42 (1953) 194–200.
- [42] E. Li, P. Funkenbusch, Experimental size ratio and compositional effects on the packing and hot isostatic pressing of spherical powders, *Mater. Sci. Eng. A* 157 (1992) 217–224.
- [43] J.T. Sims, Soil pH effects on the distribution and plant availability of manganese, copper, and zinc, *Soil Sci. Soc. Am. J.* 50 (1986) 367–373.
- [44] D. Meng, N. Zhao, M. Ma, L. Fang, Y. Gu, Y. Jia, J. Liu, W. Liu, Application of a mobile laser-induced breakdown spectroscopy system to detect heavy metal elements in soil, *Appl. Opt.* 56 (2017) 5204–5210.
- [45] A.M. Mouazen, H. Ramon, J. De Baerdemaeker, Effects of bulk density and moisture content on selected mechanical properties of sandy loam soil, *Biosyst. Eng.* 83 (2002) 217–224.
- [46] C.W. Smith, M.A. Johnston, S. Lorentz, The effect of soil compaction and soil physical properties on the mechanical resistance of South African forestry soils, *Geoderma* 78 (1997) 93–111.
- [47] C.J. Bronick, R. Lal, Soil structure and management: a review, *Geoderma* 124 (2005) 3–22.
- [48] O.S.B. Al-Amoudi, K. Khan, N.S. Al-Kahtani, Stabilization of a Saudi calcareous marl soil, *Constr. Build. Mater.* 24 (2010) 1848–1854.
- [49] A.M. Popov, A.N. Drozdova, S.M. Zaytsev, D.I. Biryukova, N.B. Zorov, T.A. Labutin, Rapid, direct determination of strontium in natural waters by laser-induced breakdown spectroscopy, *J. Anal. At. Spectrom.* 31 (2016) 1123–1130.
- [50] L.J. Prell, C. Monnig, R.E. Harris, S.R. Koirtzyhann, The role of electrons in the emission enhancement by easily ionized elements low in the inductively coupled plasma, *Spectrochim. Acta B* 40 (1985) 1401–1410.